

# Pion and kaon production in central Pb+Pb collisions at 20A and 30A GeV: Evidence for the onset of deconfinement

C. Alt,<sup>9</sup> T. Anticic,<sup>23</sup> B. Baatar,<sup>8</sup> D. Barna,<sup>4</sup> J. Bartke,<sup>6</sup> L. Betev,<sup>10</sup> H. Bialkowska,<sup>20</sup> C. Blume,<sup>9</sup> B. Boimska,<sup>20</sup> M. Botje,<sup>1</sup> J. Bracinik,<sup>3</sup> R. Bramm,<sup>7</sup> P. Bunčić,<sup>10</sup> V. Černy,<sup>3</sup> P. Christakoglou,<sup>2</sup> P. Chung,<sup>19</sup> O. Chvala,<sup>14</sup> J.G. Cramer,<sup>16</sup> P. Csató,<sup>4</sup> P. Dinkelaker,<sup>9</sup> V. Eckardt,<sup>13</sup> D. Flierl,<sup>9</sup> Z. Fodor,<sup>4</sup> P. Foka,<sup>7</sup> V. Friese,<sup>7</sup> J. Gál,<sup>4</sup> M. Gaździcki,<sup>9,11</sup> V. Genchev,<sup>18</sup> G. Georgopoulos,<sup>2</sup> E. Gladysz,<sup>6</sup> K. Grebieszkow,<sup>22</sup> S. Hegyi,<sup>4</sup> C. Höhne,<sup>12</sup> K. Kadja,<sup>23</sup> A. Karev,<sup>13</sup> D. Kikola,<sup>22</sup> M. Kliemant,<sup>9</sup> S. Kniege,<sup>9</sup> V.I. Kolesnikov,<sup>8</sup> T. Kollegger,<sup>9</sup> E. Kornas,<sup>6</sup> R. Korus,<sup>11</sup> M. Kowalski,<sup>6</sup> I. Kraus,<sup>7</sup> M. Kreps,<sup>3</sup> A. Laszlo,<sup>4</sup> R. Lacey,<sup>19</sup> M. van Leeuwen,<sup>1</sup> P. Lévai,<sup>4</sup> L. Litov,<sup>17</sup> B. Lungwitz,<sup>9</sup> M. Makarieva,<sup>17</sup> A.I. Malakhov,<sup>8</sup> M. Mateev,<sup>17</sup> G.L. Melkumov,<sup>8</sup> A. Mischke,<sup>1</sup> M. Mitrovski,<sup>9</sup> J. Molnár,<sup>4</sup> St. Mrówczyński,<sup>11</sup> V. Nicolic,<sup>23</sup> G. Pálka,<sup>4</sup> A.D. Panagiotou,<sup>2</sup> D. Panayotov,<sup>17</sup> A. Petridis,<sup>2</sup> W. Peryt,<sup>22</sup> M. Pikna,<sup>3</sup> J. Pluta,<sup>22</sup> D. Prindle,<sup>16</sup> F. Pühlhofer,<sup>12</sup> R. Renfordt,<sup>9</sup> C. Roland,<sup>5</sup> G. Roland,<sup>5</sup> M. Rybczyński,<sup>11</sup> A. Rybicki,<sup>6</sup> A. Sandoval,<sup>7</sup> N. Schmitz,<sup>13</sup> T. Schuster,<sup>9</sup> P. Seyboth,<sup>13</sup> F. Siklér,<sup>4</sup> B. Sitar,<sup>3</sup> E. Skrzypczak,<sup>21</sup> M. Slodkowski,<sup>22</sup> G. Stefanek,<sup>11</sup> R. Stock,<sup>9</sup> C. Strabel,<sup>9</sup> H. Ströbele,<sup>9</sup> T. Susa,<sup>23</sup> I. Szentpéteri,<sup>4</sup> J. Sziklai,<sup>4</sup> M. Szuba,<sup>22</sup> P. Szymanski,<sup>20</sup> V. Trubnikov,<sup>20</sup> D. Varga,<sup>4</sup> M. Vassiliou,<sup>2</sup> G.I. Veres,<sup>4</sup> G. Vesztregombi,<sup>4</sup> D. Vranić,<sup>7</sup> A. Wetzler,<sup>9</sup> Z. Włodarczyk,<sup>11</sup> I.K. Yoo,<sup>15</sup> and J. Zimányi<sup>\*4</sup>

(The NA49 collaboration)

<sup>1</sup>NIKHEF, Amsterdam, Netherlands.

<sup>2</sup>Department of Physics, University of Athens, Athens, Greece.

<sup>3</sup>Comenius University, Bratislava, Slovakia.

<sup>4</sup>KFKI Research Institute for Particle and Nuclear Physics, Budapest, Hungary.

<sup>5</sup>MIT, Cambridge, USA.

<sup>6</sup>Henryk Niewodniczanski Institute of Nuclear Physics, Polish Academy of Science, Cracow, Poland.

<sup>7</sup>Gesellschaft für Schwerionenforschung (GSI), Darmstadt, Germany.

<sup>8</sup>Joint Institute for Nuclear Research, Dubna, Russia.

<sup>9</sup>Fachbereich Physik der Universität, Frankfurt, Germany.

<sup>10</sup>CERN, Geneva, Switzerland.

<sup>11</sup>Institute of Physics Świątkrzyska Academy, Kielce, Poland.

<sup>12</sup>Fachbereich Physik der Universität, Marburg, Germany.

<sup>13</sup>Max-Planck-Institut für Physik, Munich, Germany.

<sup>14</sup>Institute of Particle and Nuclear Physics, Charles University, Prague, Czech Republic.

<sup>15</sup>Department of Physics, Pusan National University, Pusan, Republic of Korea.

<sup>16</sup>Nuclear Physics Laboratory, University of Washington, Seattle, WA, USA.

<sup>17</sup>Atomic Physics Department, Sofia University St. Kliment Ohridski, Sofia, Bulgaria.

<sup>18</sup>Institute for Nuclear Research and Nuclear Energy, Sofia, Bulgaria.

<sup>19</sup>Department of Chemistry, Stony Brook University (SUNYSB), Stony Brook, USA.

<sup>20</sup>Institute for Nuclear Studies, Warsaw, Poland.

<sup>21</sup>Institute for Experimental Physics, University of Warsaw, Warsaw, Poland.

<sup>22</sup>Faculty of Physics, Warsaw University of Technology, Warsaw, Poland.

<sup>23</sup>Rudjer Boskovic Institute, Zagreb, Croatia.

Results on charged pion and kaon production in central Pb+Pb collisions at 20A and 30A GeV are presented and compared to data at lower and higher energies. A rapid change of the energy dependence is observed around 30A GeV for the yields of pions and kaons as well as for the shape of the transverse mass spectra. The change is compatible with the prediction that the threshold for production of a state of deconfined matter at the early stage of the collisions is located at low SPS energies.

PACS numbers: 25.75.-q

## INTRODUCTION

The advent of the quark model of hadrons and the development of quantum chromodynamics naturally led to the question whether strongly interacting matter exists in different phases and, if so, of which nature the transitions

---

\* deceased

between these phases are. In particular, it is commonly believed that a gas of hadrons will undergo a transition to a state of quasi-free quarks and gluons, the Quark Gluon Plasma (QGP) [1], when its temperature exceeds a critical value [2]. These questions have motivated a broad experimental program of nucleus-nucleus collisions to study the properties of strongly interacting matter at extreme densities and temperatures.

Several signatures of the formation of a transient QGP state during the early stage of a nucleus-nucleus collision at high energies were proposed in the past [3]. However, the validity of these signatures has come under renewed scrutiny. For this reason the NA49 Collaboration at the CERN SPS has searched over the past years for signs of the onset of QGP creation in the energy dependence of hadron production. This search was motivated by the prediction of [4, 5, 6] that the onset of deconfinement should lead to a steepening of the increase of the pion yield with collision energy and to a sharp maximum in the energy dependence of the strangeness to pion ratio. The onset was expected to occur at approximately 30A GeV [6].

The NA49 energy scan program at the CERN SPS started with two runs where data on central Pb+Pb collisions at 40A and 80A GeV were recorded in 1999 and 2000. Data at the top SPS energy of 158A GeV had already been taken in previous SPS runs. The analysis of these runs was published in [7] and the results confirmed the predictions of [6]. This finding motivated an extension of the energy scan to the lower SPS energies of 30A and 20A GeV which was completed in 2002. In this letter we report final results on charged kaon and pion production in central Pb+Pb collisions at 20A and 30A GeV beam energy. The present measurements are combined with those from [7] and compared to available model calculations, together with lower and higher energy data from AGS and RHIC.

## DETECTOR AND DATA ANALYSIS

The NA49 experimental set-up [8] consists of four large volume Time Projection Chambers (TPC). Two of these (VTPC) are placed in the field of two super-conducting dipole magnets. The other two TPCs (MTPC) are positioned downstream of the magnets and are optimized for high precision measurements of the ionization energy loss  $dE/dx$  with a resolution of about 4%. This  $dE/dx$  measurement provides particle identification which is complemented by a measurement of the time-of-flight (TOF) with a resolution of about 60 ps in two TOF detector arrays positioned downstream of the MTPCs. At each incident energy the TOF acceptance for kaons was kept at mid-rapidity by lowering in proportion to the beam energy the nominal 158A GeV field settings of about 1.5 (upstream magnet) and 1.1 T (downstream magnet). In both the 30A and 20A GeV runs a thin lead foil target of 224 mg/cm<sup>2</sup>, corresponding to about 1% of interaction length for Pb ions, was positioned 80 cm upstream from the first TPC. A trigger based on a measurement of the energy deposit of projectile spectator nucleons in a downstream calorimeter selected the most central 7.2% of the Pb+Pb collisions. The corresponding mean number of wounded nucleons  $N_w$  [9] is calculated using the Fritiof model [10] to be  $N_w = 349 \pm 1(\text{stat}) \pm 5(\text{sys})$ . At each energy about  $3.5 \times 10^5$  events were recorded.

Results on kaon and pion production were obtained in a multi-step analysis procedure which involves charged track reconstruction, particle identification and corrections to account for background contributions as well as for acceptance and efficiency losses. To reduce the systematic errors, the analysis has been restricted to regions of phase space where background and efficiency corrections are small and approximately uniform. To minimize tracking efficiency corrections, only tracks within an azimuthal angle wedge of  $\pm 30^\circ$  with respect to the horizontal plane were used.

The spectra of  $\pi^\pm$  and  $K^\pm$  at mid-rapidity are obtained using the combined  $dE/dx$  and TOF information as described in [11] (TOF +  $dE/dx$  analysis). The pion spectra were corrected for the contribution from the weak decays of the strange particles  $\Lambda$ ,  $\Sigma^0$ ,  $\Sigma^\pm$  and  $K_S^0$  as well as for  $\mu$  contamination (charged products of weak decays can be reconstructed as coming from the event interaction vertex, while muons cannot be separated from pions in NA49 with  $dE/dx$  and TOF measurements for momenta above about 1 GeV/c). The correction factors were obtained from a GEANT simulation of the NA49 detector using as input the hadron distributions from the VENUS model [12]. The model distributions were tuned to reproduce the measured yields of  $\Lambda$  [13] and  $K_S^0$  where the latter were taken to be the average of the  $K^\pm$  yields presented in this paper. The total background correction to the  $\pi^-$  ( $\pi^+$ ) yields is found to be about 8 (6)%.

Raw  $K^+$  and  $K^-$  yields at forward rapidities were extracted from fits of the  $dE/dx$  distributions in narrow bins of momentum and transverse momentum. The fitted function parametrizes contributions from  $e^+$ ,  $\pi^+$ ,  $K^+$ , protons and deuterons to the  $dE/dx$  spectra of positively charged particles and corresponding contributions to those of negatively charged particles. For pions the  $dE/dx$  method does not provide sufficiently accurate identification in the low  $p_T$  region near mid-rapidity. Therefore to obtain the raw  $\pi^-$  spectra in the full forward hemisphere of the reactions yields of all negatively charged particles were determined as a function of rapidity (calculated assuming the pion mass) and transverse momentum  $p_T$ . The contamination by  $K^-$ ,  $\bar{p}$  and  $e^-$  from the interaction vertex as well as

non-vertex hadrons originating from strange particle decays and secondary interactions was subtracted. The total correction amounts to 20-25% and was calculated using the VENUS/GEANT simulation. The above procedure can not be applied for positively charged hadrons due to the large contribution of kaons and protons.

The resulting background subtracted spectra were corrected for geometrical acceptance, losses due to in-flight decays, inefficiencies of the tracking algorithms (about 5%) and quality cuts. More details on the correction procedure can be found in [7].

Systematic errors were estimated by comparing results obtained with different detectors (TPC, TOF) and by varying cuts and correction strategies. Uncertainties in the parameters of the  $dE/dx$  fits lead to asymmetric systematic errors on the kaon yields. The systematic errors were estimated to be 5-10% and are explicitly given in Table II. Note that to a large extent the systematic uncertainties presented here are common to those reported in [7] since there the same experimental procedure was used.

## RESULTS AT 20A AND 30A GEV

In Fig. 1 are shown the transverse mass spectra of  $\pi^\pm$  mesons near mid-rapidity  $0 < y < 0.2$  together with those

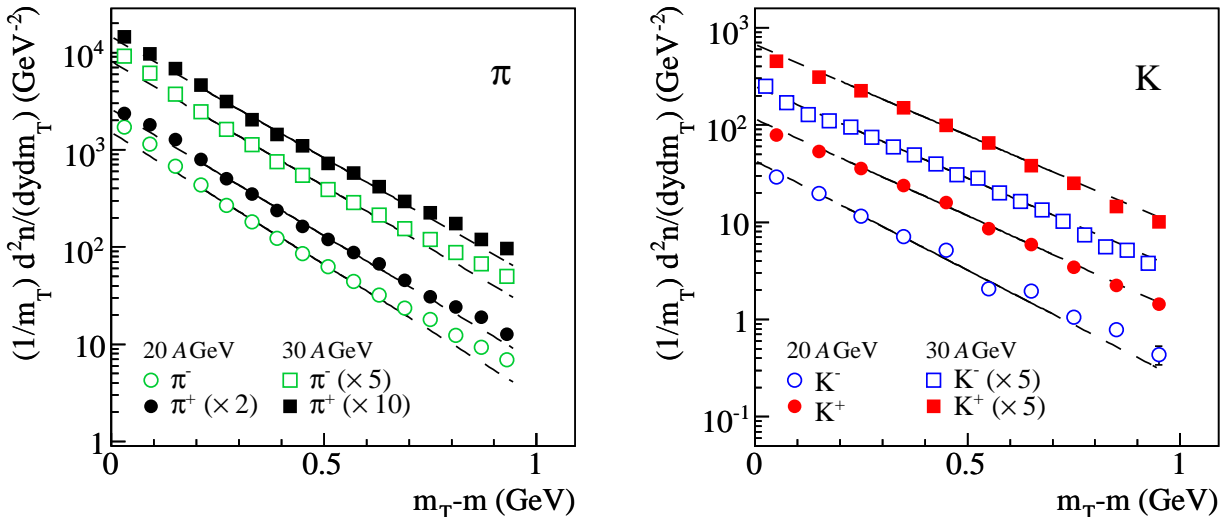


FIG. 1: Transverse mass spectra of  $\pi^-$  and  $\pi^+$  mesons at  $0 < y < 0.2$  (left) and those of  $K^+$  and  $K^-$  mesons at  $|y| < 0.1$  (right) produced in central Pb+Pb collisions at 20A and 30A GeV. The lines are fits of Eq. (1) to the spectra in the interval  $0.2 < m_T - m < 0.7$  GeV. The statistical errors are smaller than the symbol size. The systematic errors are 5% in the region used for the fit and reach 10% at the low and high ends of the  $m_T$  spectra.

of  $K^\pm$  at  $|y| < 0.1$  obtained from the TOF +  $dE/dx$  analysis of 20A and 30A GeV central Pb+Pb collisions. Here the transverse mass is defined by  $m_T^2 = p_T^2 + m^2$  with  $m$  the rest mass of the particle, and  $y$  denotes the rapidity of a particle in the collision center-of-mass system. The full lines in Fig. 1 indicate a fit of the function

$$\frac{d^2n}{m_T dm_T dy} = C \exp\left(-\frac{m_T}{T}\right) \quad (1)$$

to the data in the range  $0.2 < m_T - m < 0.7$  GeV. The values obtained for the inverse slope parameter  $T$  are given in Table I.

The kaon spectra are well described by the fit, while the low and high  $m_T$  regions of the pion spectra outside of the fitted region are above the extrapolated fitted line.

The rapidity distributions  $dn/dy$  of  $\pi^-$ ,  $K^-$  and  $K^+$  mesons are plotted in Fig. 2. These distributions were obtained by summing the measured  $m_T$  spectra and using the fitted exponential function Eq. (1) to extrapolate to full  $m_T$ . For kaons the corresponding corrections are below 10% for most of the rapidity bins except for the first two and the last rapidity bin from the  $dE/dx$  only analysis in which not more than about 50% of the yield is in the measured

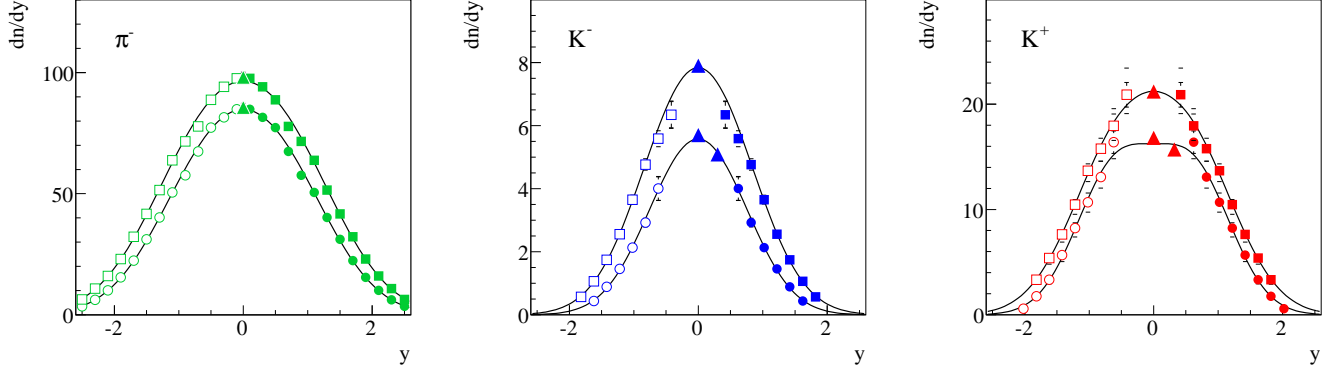


FIG. 2: Rapidity distributions of  $\pi^-$  (left),  $K^-$  (middle) and  $K^+$  mesons (right) produced in central  $Pb+Pb$  collisions at  $20A$  (lower curves) and  $30A$  GeV (upper curves). Squares and circles show the results of an analysis based on  $dE/dx$  only whereas triangles are obtained from a  $TOF + dE/dx$  analysis. The closed symbols indicate measured points while the open points are reflected with respect to mid-rapidity. The lines indicate fits of Eq. (2) to the data. The errors, which are often smaller than the symbol size, are statistical only. The systematic errors on the measurements are about  $\pm 5\%$ .

region. The corrections for pions are negligible. The rapidity spectra were parameterized by the sum of two Gaussian distributions positioned symmetrically with respect to mid-rapidity [7]

$$\frac{dn}{dy} = \frac{\langle n \rangle}{2\sqrt{2\pi}\sigma} \left\{ \exp \left[ -\frac{1}{2} \left( \frac{y - y_0}{\sigma} \right)^2 \right] + \exp \left[ -\frac{1}{2} \left( \frac{y + y_0}{\sigma} \right)^2 \right] \right\}, \quad (2)$$

where  $\langle n \rangle$ ,  $\sigma$  and  $y_0$  are fit parameters. The results of the fits are indicated by the full lines in Fig. 2 and the values of the parameters are given in Table I. Also given in this Table are the mean multiplicities which were obtained by integration of the fitted curves and the mid-rapidity yields that were taken to be the maxima of the curves. The

TABLE I: In the columns on the left are listed the inverse slope parameters  $T$  obtained from a fit of Eq. (1) to the  $m_T$  spectra at mid-rapidity, together with the parameters  $\sigma$  and  $y_0$  from a fit of Eq. (2) to the  $\pi^-$  and  $K^\pm$  rapidity spectra. Only statistical errors are given. The values of  $\sigma$  and  $y_0$  are significantly correlated. In the columns on the right are listed the full phase space yields  $\langle \pi^\pm \rangle$  and  $\langle K^\pm \rangle$  together with  $dn/dy$  for  $\pi^\pm$  and  $K^\pm$  production at mid-rapidity. The first error is statistical, the second systematic. Note that  $\langle \pi^+ \rangle$  is not directly measured (see text).

Parameter	$20A$ GeV	$30A$ GeV	Yield	$20A$ GeV	$30A$ GeV
$T(\pi^+)$ (MeV)	$167 \pm 2$	$175 \pm 2$	$\langle \pi^- \rangle$	$221 \pm 1 \pm 11$	$274 \pm 1 \pm 14$
$T(\pi^-)$ (MeV)	$160 \pm 2$	$169 \pm 2$	$\langle \pi^+ \rangle$	$190 \pm 1 \pm 9$	$241 \pm 1 \pm 12$
$T(K^+)$ (MeV)	$219 \pm 5$	$232 \pm 5$	$\langle K^+ \rangle$	$40.7 \pm 0.7 \pm 2.2$	$52.9 \pm 0.9^{+3.0}_{-3.5}$
$T(K^-)$ (MeV)	$193 \pm 9$	$230 \pm 7$	$\langle K^- \rangle$	$10.3 \pm 0.1 \pm 0.2$	$16.0 \pm 0.2 \pm 0.4$
$\sigma(\pi^-)$	$0.837 \pm 0.007$	$0.885 \pm 0.007$	$dn/dy(\pi^-)$	$84.8 \pm 0.4 \pm 4.2$	$96.5 \pm 0.5 \pm 4.8$
$\sigma(K^+)$	$0.601 \pm 0.012$	$0.722 \pm 0.026$	$dn/dy(\pi^+)$	$72.9 \pm 0.3 \pm 3.6$	$83.0 \pm 0.4 \pm 4.2$
$\sigma(K^-)$	$0.642 \pm 0.035$	$0.710 \pm 0.032$	$dn/dy(K^-)$	$5.58 \pm 0.07 \pm 0.11$	$7.8 \pm 0.1 \pm 0.2$
$y_0(\pi^-)$	$0.557 \pm 0.009$	$0.624 \pm 0.009$	$dn/dy(K^+)$	$16.4 \pm 0.6 \pm 0.4$	$21.2 \pm 0.8^{+1.5}_{-0.9}$
$y_0(K^+)$	$0.606 \pm 0.014$	$0.578 \pm 0.030$			
$y_0(K^-)$	$0.34 \pm 0.06$	$0.37 \pm 0.05$			

mean multiplicity of  $\pi^+$  mesons and their mid-rapidity yields were calculated by scaling  $\langle \pi^- \rangle$  with the  $\pi^+/\pi^-$  ratio measured at mid-rapidity in the  $TOF + dE/dx$  analysis. These ratios were found to be  $(0.86, 0.88, 0.90, 0.91, 0.93)$  for the data measured at  $(20, 30, 40, 80, 158)A$  GeV. The ratios at the latter three energies were used to recalculate the published values of the  $\langle \pi^+ \rangle$  and the  $\pi^+$  mid-rapidity yields at these energies. The recalculated  $\pi^+$  multiplicities differ by several percent from the ones published in [7].

## REVIEW OF THE ENERGY DEPENDENCE

In this section, the new results on  $\pi$  and K production at  $20A$  and  $30A$  GeV will be discussed together with published measurements at lower (AGS) and higher (SPS, RHIC) energies and compared to the corresponding data from  $p + p(\bar{p})$  interactions. Model calculations, which are shown by the curves in the figures below, will be discussed in the next section.

In Fig. 3 is shown the mean pion multiplicity  $\langle \pi \rangle = 1.5 (\langle \pi^+ \rangle + \langle \pi^- \rangle)$  per wounded nucleon  $\langle N_w \rangle$  as a function of

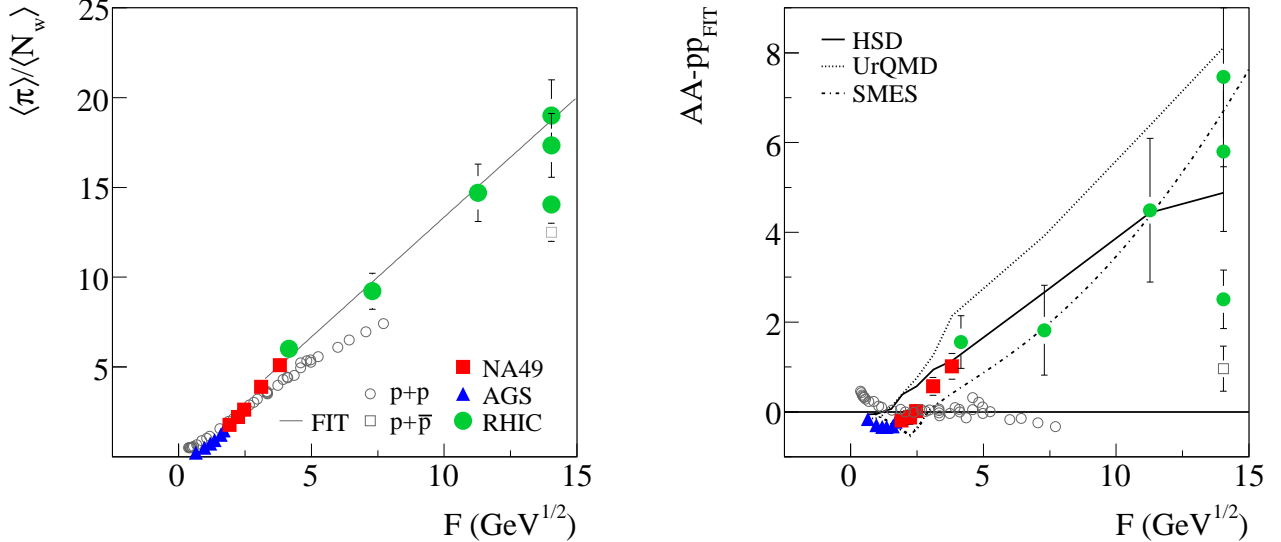


FIG. 3: Left: Energy dependence of the mean pion multiplicity per wounded nucleon measured in central Pb+Pb and Au+Au [15, 16] collisions (full symbols), compared to the corresponding results from  $p + p(\bar{p})$  reactions (open circles). Right: Energy dependence of the difference between the measured mean pion multiplicity per wounded nucleon and a parametrization (see text) of the  $p + p$  data. The meaning of the full and open symbols is the same as in the left-hand plot. The lines show various model predictions described in the text.

the collision energy, expressed by Fermi's measure [14]

$$F \equiv \left[ \frac{(\sqrt{s_{NN}} - 2m_N)^3}{\sqrt{s_{NN}}} \right]^{1/4},$$

where  $\sqrt{s_{NN}}$  is the centre-of-mass energy per nucleon-nucleon pair and  $m_N$  the nucleon rest mass. The use of  $F$  in Fig. 3 is motivated by model expectations, as will be discussed below.

In Fig. 3 the measurements by NA49 are compared to results from the AGS [15] and RHIC [16] on central nucleus-nucleus collisions. The lowest point at the top RHIC energy is obtained from the BRAHMS measurements of identified hadron spectra. The middle and highest points are results from, respectively, BRAHMS and PHOBOS on the charged hadron mean multiplicity corrected for non-pion contributions by use of the BRAHMS identified hadron yields. The RHIC points at the lower energies are from PHOBOS, again corrected for the non-pion contribution. The results from  $p + p(\bar{p})$  interactions are shown by the open symbols. For ease of comparison these data were fitted to the parameterization

$$\frac{\langle \pi \rangle}{\langle N_w \rangle} = a + b F + c F^2, \quad (3)$$

resulting in  $a = -0.44 \pm 0.06$ ,  $b = 1.32 \pm 0.03$  GeV $^{-1/2}$  and  $c = -0.033 \pm 0.004$  GeV $^{-1}$ . Up to the top SPS energy the mean pion multiplicity in  $p + p$  interactions is approximately proportional to  $F$ . A fit of Eq. (3) in the range  $2 < F < 5$  GeV $^{1/2}$  with  $a = c = 0$  yielded a value of  $b = 1.063 \pm 0.003$  GeV $^{-1/2}$ .

For central Pb+Pb and Au+Au collisions the energy dependence is more complicated as is seen in the right panel of Fig. 3 where the difference between the data and the  $p + p$  parameterization Eq. (3) is plotted. Below 40A GeV the

ratio  $\langle \pi \rangle / \langle N_w \rangle$  is lower in A+A collisions than in p+p interactions (pion suppression) while at higher energies this ratio is larger in A+A collisions than in p + p interactions (pion enhancement). The transition from pion suppression to pion enhancement is clearly demonstrated in the figure. A linear fit for  $F < 1.85 \text{ GeV}^{1/2}$  using Eq. (3) with  $c = 0$  gave  $a = -0.45 \pm 0.05$  and  $b = 1.03 \pm 0.05 \text{ GeV}^{-1/2}$ . The slope parameter fitted in the range  $F > 3.5 \text{ GeV}^{1/2}$  was  $b = 1.33 \pm 0.03$  where the lowest point at the top RHIC energy was excluded from the fit. Thus, in the region 15–40A GeV between the highest AGS and the lowest SPS energy the slope increases by a factor of about 1.3.

Fig. 4 shows the full phase space ratios  $\langle K^+ \rangle / \langle \pi^+ \rangle$  and  $E_S = (\langle \Lambda \rangle + \langle K + \bar{K} \rangle) / \langle \pi \rangle$  as a function of collision energy

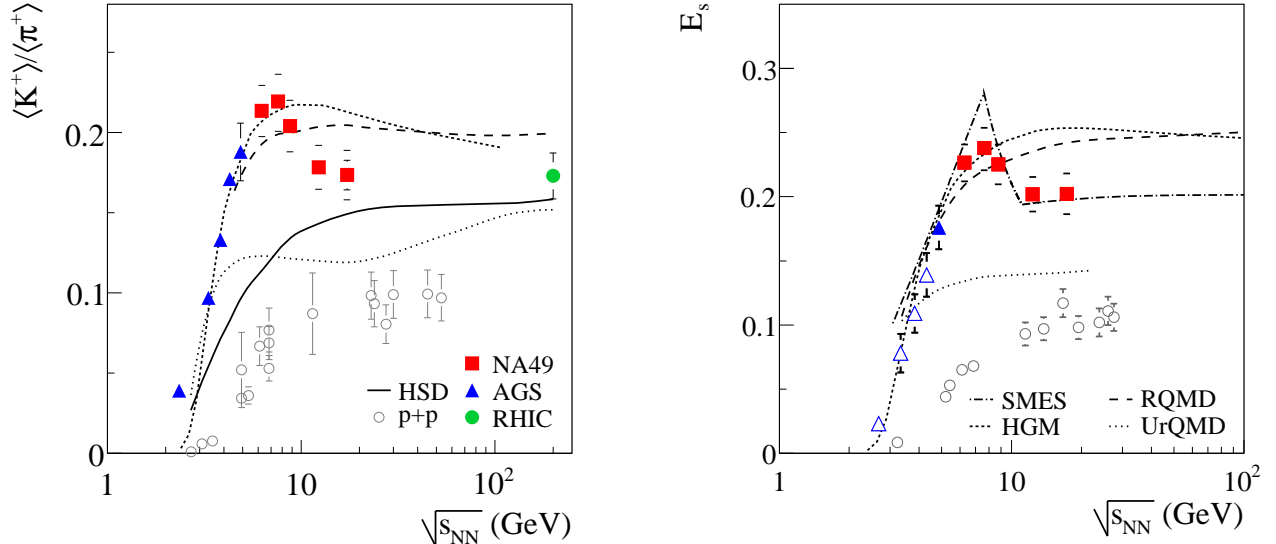


FIG. 4: Left: Energy dependence of the  $\langle K^+ \rangle / \langle \pi^+ \rangle$  ratio measured in central Pb+Pb and Au+Au [15, 16] collisions (full symbols) compared to the corresponding results from p+p( $\bar{p}$ ) reactions (open circles). Right: Energy dependence of the relative strangeness production as measured by the  $E_S$  ratio (see text) in central Pb+Pb and Au+Au collisions (full symbols) compared to results from p + p( $\bar{p}$ ) reactions (open circles). The curves in the figures show predictions of various models described in the text.

in the left and right panels, respectively. Kaons are the lightest strange hadrons and  $\langle K^+ \rangle$  accounts for about half of all the anti-strange quarks produced in Pb+Pb collisions at AGS and SPS energies (a detailed explanation is given below). In the  $E_S$  ratio all main carriers of strange and anti-strange quarks are included. The values for Pb+Pb and Au+Au collisions were calculated using data from this paper and Refs. [7, 15, 17, 18]. The neglected contribution of  $\bar{\Lambda}$  and other hyperons and anti-hyperons is about 10% at SPS energies. Both the  $\langle K^+ \rangle / \langle \pi^+ \rangle$  and  $E_S$  ratios are approximately, within 5% at SPS energies, proportional to the ratio of total multiplicity of  $s$  and  $\bar{s}$  quarks to the multiplicity of pions. It should be noted that the  $\langle K^+ \rangle / \langle \pi^+ \rangle$  ratio is expected to be similar (within about 10%) for p + p, n + p and n + n interactions at 158A GeV [19], whereas the  $E_S$  ratio is independent of the isospin of nucleon-nucleon interactions. Calculating the  $E_S$  ratio for the p + p data [4] is significantly more precise than taking the ratio  $\langle K^+ \rangle / \langle \pi^+ \rangle$ .

It is seen from Fig. 4 that a steep increase of both ratios in the AGS energy region is followed by a turnover and a decrease around 30A GeV. The BRAHMS measurements at the top RHIC energy [16] indicate that the  $\langle K^+ \rangle / \langle \pi^+ \rangle$  ratio stays nearly constant starting from the top SPS energy. The RHIC results for the  $E_S$  ratio are not available because the total multiplicity of  $\Lambda$  hyperons is not measured. For comparison the results from p + p interactions [4] are also plotted in Fig. 4. These data show a monotonic increase with increasing energy.

The ratios  $\langle K^- \rangle / \langle \pi^- \rangle$  and  $K^- / K^+$  at mid-rapidity (see below for details) increase monotonically with increasing collision energy, as can be seen from Fig. 5. The difference between the dependence of the  $K^+$  and  $K^-$  yields on collision energy can be attributed to their different sensitivity to the baryon density.  $K^+$  and  $K^0$  carry a dominant fraction of all produced  $\bar{s}$ -quarks exceeding 95% in Pb+Pb collisions at 158A GeV if open strangeness is considered. Because  $\langle K^+ \rangle \cong \langle K^0 \rangle$  in approximately isospin symmetric collisions of heavy nuclei, the  $K^+$  yield is nearly proportional to the total strangeness production and only weakly sensitive to the baryon density. As a significant fraction of  $s$ -quarks (about 50% in central Pb+Pb collisions at 158A GeV) is carried by hyperons, the number of produced anti-kaons

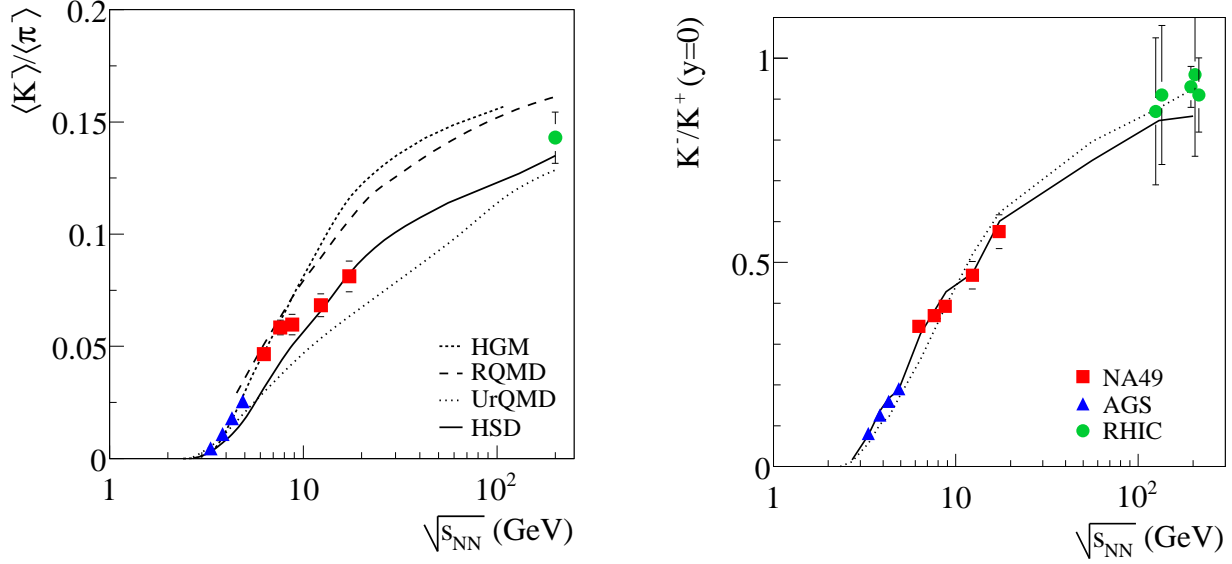


FIG. 5: Left: Energy dependence of the ratio  $\langle K^- \rangle / \langle \pi^- \rangle$  measured in central Pb+Pb and Au+Au [15, 16] collisions (full symbols). Right: Energy dependence of the ratio of mid-rapidity yields of  $K^-$  and  $K^+$  mesons. The curves in the figures show model predictions described in the text.

$K^-$  and  $\bar{K}^0$  is sensitive to both the strangeness yield and the baryon density.

In Fig. 6 the mid-rapidity ratios  $K^+/\pi^+$  and  $K^-/\pi^-$  for central Pb+Pb and Au+Au collisions are shown as a

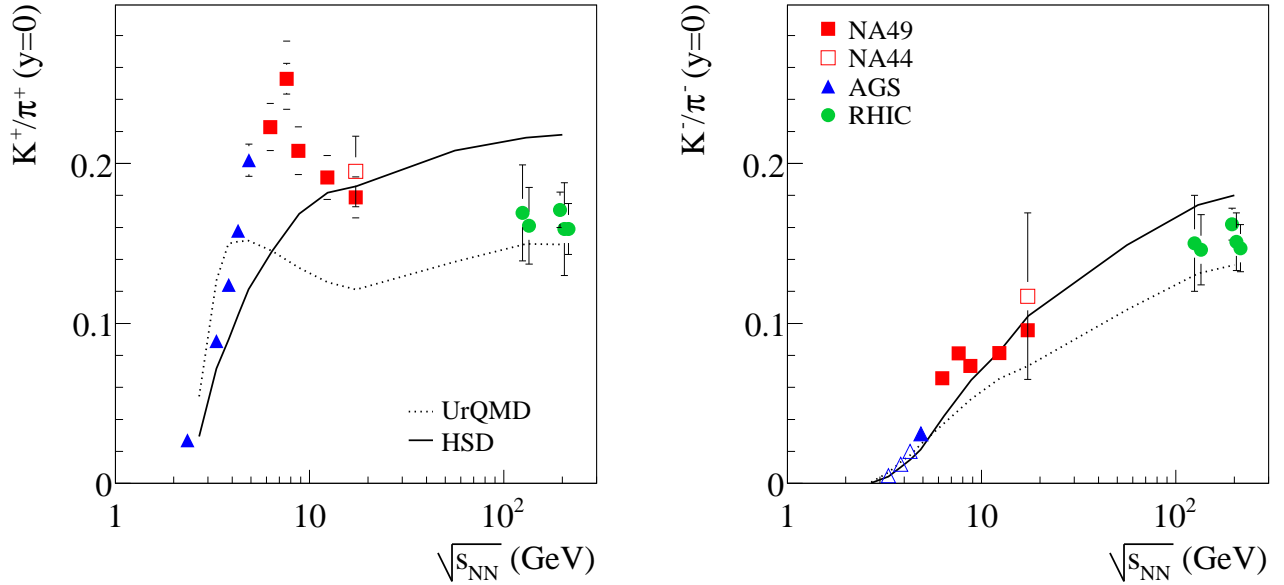


FIG. 6: Energy dependence of the ratio  $K^+/\pi^+$  (left) and  $K^-/\pi^-$  (right) at mid-rapidity measured in central Pb+Pb and Au+Au [15, 16] collisions. The NA44 data are taken from [20].

function of the collision energy. All NA49 mid-rapidity results presented here are determined from the fits of the rapidity spectra to Eq. (2). The statistical and systematic errors were calculated taking into account all correlations between the fitted parameters. It is seen from Fig. 6 that the NA44 data point [20] is consistent with the NA49 results and that the STAR and PHENIX measurements at the top RHIC energies are in agreement with the trend

seen in the SPS results. Comparison with the left-hand plots of Fig. 4 and 5 shows that the energy dependence of the mid-rapidity kaon to pion ratios is similar to that of the corresponding ratios measured in full phase-space.

Fig. 7 presents the energy dependence of the inverse slope parameter  $T$  of the transverse mass spectra of  $K^+$  (left

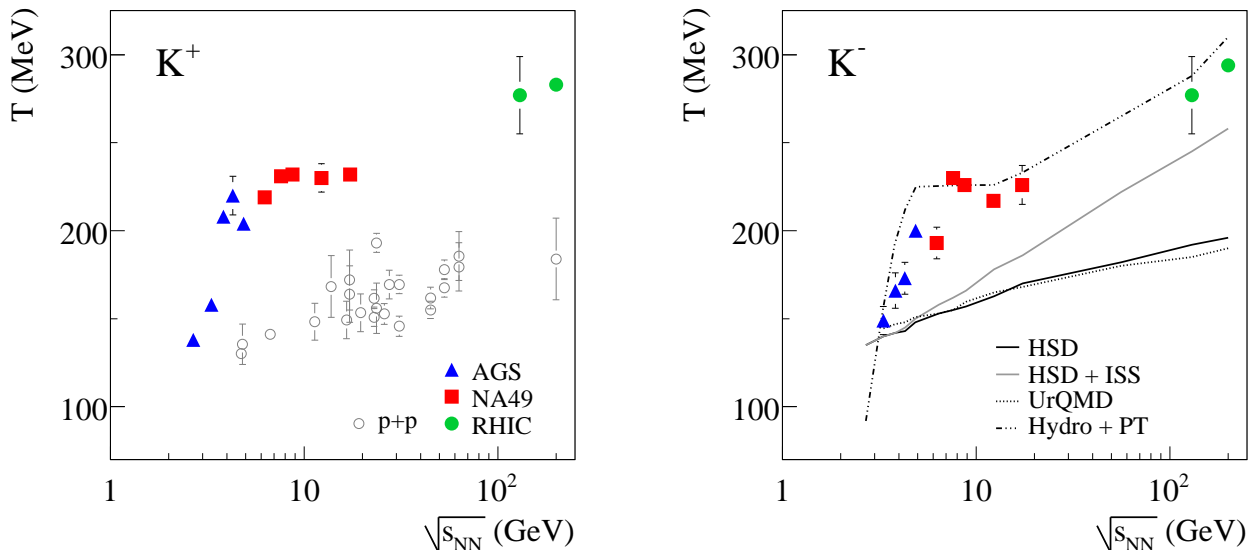


FIG. 7: Energy dependence of the inverse slope parameter  $T$  of the transverse mass spectra of  $K^+$  (left) and  $K^-$  mesons (right) measured at mid-rapidity in central Pb+Pb and Au+Au [15, 16] collisions. The  $K^+$  slope parameters are compared to those from  $p + p(\bar{p})$  reactions [21] in the left-hand plot (open circles). The curves in the right-hand plot represent predictions from various models described in the text.

panel) and  $K^-$  mesons (right panel) produced in central Pb+Pb and Au+Au collisions. One observes a plateau at SPS energies which is preceded by a steep rise of  $T$  measured at the AGS [15] and followed by an indication of a further increase of the RHIC data [16]. Although the scatter of data points is large,  $T$  appears to increase smoothly in  $p + p(\bar{p})$  interactions [21] as shown in the left panel of Fig. 7.

The transverse mass spectra of pions and protons are non-exponential such that the inverse slope parameter depends on the transverse mass interval used in the fit. The mean transverse mass  $\langle m_T \rangle - m$  provides an alternative characterization of the  $m_T$  spectra that avoids this problem. It was calculated from multi-parameter fits to the measured data in the interval  $m_T - m \leq 2.0$  GeV. For pions either a sum of two exponentials or a power law function was used, which both yield a good description of the data. In case of kaons either a single exponential or a power law was used. The final  $\langle m_T \rangle - m$  values are the average of the result from both fit methods. The error is the quadratic sum of the statistical error and a systematic contribution that is estimated from the differences in the results obtained with the two different fit functions. The values of  $\langle m_T \rangle$  at AGS and RHIC energies were calculated from the spectra published in [15, 16]. The measurements of  $\langle m_T \rangle$  for  $p$  and  $\bar{p}$  at the SPS were taken from [22]. The energy dependence of  $\langle m_T \rangle$  for pions, kaons and protons is shown in Fig. 8. The results show that the approximate energy independence of  $\langle m_T \rangle$  in the SPS energy range is a common feature for all particles investigated.

In conclusion, rapid changes in the energy dependence of pion and kaon production properties are observed which all seem to coincide in the low SPS energy range of 20–30A GeV. This suggests that a common underlying physics process is responsible for these changes.

## DISCUSSION OF MODEL EXPLANATIONS

In this section the energy dependence of pion and strangeness production properties will be discussed within various approaches to nucleus-nucleus collisions and compared with published model predictions.

It was suggested in [4, 5] that a transition to a deconfined state of matter may cause anomalies in the energy dependence of pion and strangeness production in nucleus-nucleus collisions. This led to the formulation of the Statistical Model of the Early Stage (SMES) [5, 6] which is based on the assumption that the system created at the

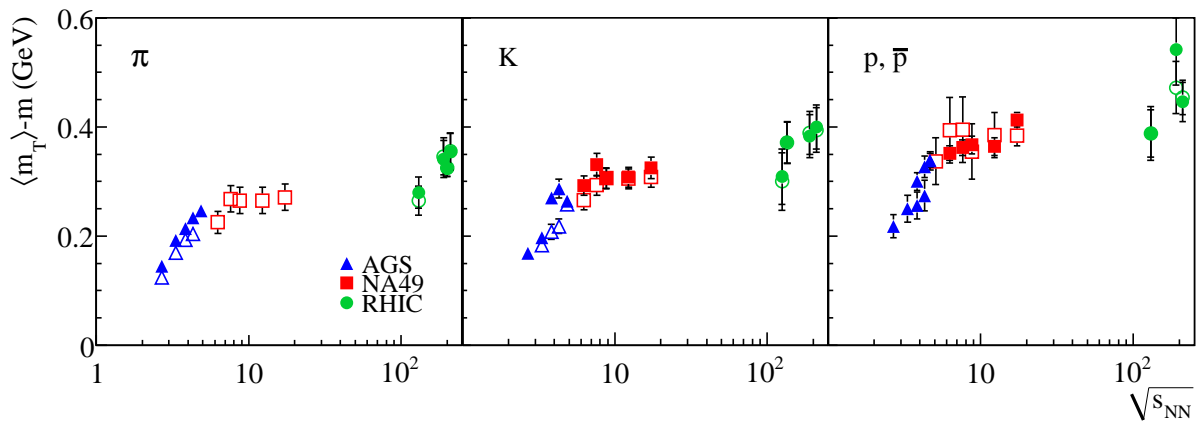


FIG. 8: Energy dependence of the mean transverse mass  $\langle m_T \rangle$  measured at mid-rapidity in central Pb+Pb and Au+Au collisions for  $\pi^\pm$  (left) and  $K^\pm$  (middle). For completeness, the previously published results on p and  $\bar{p}$  [22] are shown in the right panel. In the plots, positively (negatively) charged hadrons are indicated by the full (open) symbols. The results from AGS and RHIC are taken from [15, 16].

early stage (be it confined matter or a QGP) is in equilibrium and that a transition from a reaction with purely confined matter to a reaction with a QGP at the early stage occurs when the transition temperature  $T_c$  is reached. For  $T_c$  values of 170–200 MeV the transition region extends from  $15A$  to  $60A$  GeV [6]. Assuming the generalized Fermi-Landau conditions [6, 14, 23] for the early stage of nucleus-nucleus collisions and a proportionality of the pion multiplicity to the early stage entropy, the ratio  $\langle \pi \rangle / \langle N_w \rangle$  increases linearly with the Fermi measure  $F$  outside the transition region. The slope parameter is proportional to  $g^{1/4}$  [5], where  $g$  is the effective number of internal degrees of freedom at the early stage. In the transition region a steepening of the pion energy dependence is due to the activation of a large number of partonic degrees of freedom. This is, in fact, observed in the data on central Pb+Pb and Au+Au collisions, where the steepening starts at about  $20A$  GeV, as shown in Fig. 3. The linear dependence of  $\langle \pi \rangle / \langle N_w \rangle$  on  $F$  is approximately obeyed by the data at lower and higher energies (including RHIC). An increase of the slope by a factor of about 1.3 is measured, which corresponds to an increase of the effective number of internal degrees of freedom by a factor of  $1.3^4 \cong 3$ , within the SMES [5].

The  $\langle K^+ \rangle / \langle \pi^+ \rangle$  and  $E_S$  ratios are roughly proportional to the total strangeness to entropy ratio which in the SMES model is assumed to be preserved from the early stage till freeze-out. At low collision energies the strangeness to entropy ratio increases steeply with collision energy, due to the low temperature at the early stage ( $T < T_c$ ) and the high mass of the strangeness carriers in the confined state (the kaon mass, for instance, is 500 MeV). When the transition to a QGP is crossed ( $T > T_c$ ), the mass of the strangeness carriers is significantly reduced to the strange quark mass of about 100 MeV. Due to the low mass  $m < T$ , the strangeness yield becomes (approximately) proportional to the entropy, and the strangeness to entropy (or pion) ratio is independent of energy. This leads to a decrease in the energy dependence from the larger value for confined matter at  $T_c$  to the QGP value. Thus the measured non-monotonic energy dependence of the strangeness to entropy ratio is followed by a saturation at the QGP value. Such anomalous energy dependence can indeed be seen in Fig. 4 and is, within the SMES, a direct consequence of the onset of deconfinement taking place at about  $30A$  GeV.

In the mixed phase region the early stage pressure and temperature are independent of the energy density [24]. Consequently, within the SMES model this should lead to the weakening of the increase with energy of the inverse slope parameter  $T$  or, equivalently, the mean transverse mass  $\langle m_T \rangle$  in the SPS energy range [25]. This qualitative prediction is confirmed by the results shown in Figs. 7 and 8. Moreover, recent hydrodynamic calculations [26] that model both the deconfined and hadronic phases provide a quantitative description of the data as shown by the dashed-dotted curve in Fig. 7.

Several other analyses of the energy dependence of hadron production properties in central Pb+Pb and Au+Au collisions within various theoretical approaches support the hypothesis that the onset of deconfinement is located at the low SPS energies. In particular such a result was obtained from studies of hadron yields within a non-equilibrium hadron gas model [27] and using the momentum integrated Boltzmann equation for a description of the time evolution of the relative strangeness yield [28]. Furthermore it was deduced from the experimentally measured rapidity spectra that within Landau's hydrodynamical model the sound velocity at the early stage of the reaction has a minimum at about  $30A$  GeV [29]. A minimum of the sound velocity is expected to occur in the phase transition domain. Moreover,

a simultaneous analysis of the two-pion correlation function and the transverse mass spectra found a plateau in the averaged phase-space density at SPS energies which may be associated with the onset of deconfinement [30].

Numerous models have been developed to explain hadron production in reactions of heavy nuclei without explicitly invoking a transient QGP phase. The simplest one is the statistical hadron gas model [31] where independent of the collision energy the hydrochemical freeze-out creates a hadron gas in equilibrium. The temperature, the baryon chemical potential and the hadronization volume are free parameters of the model and are fitted to the data at each energy. In this formulation, the hadron gas model cannot predict the energy dependence of hadron production so that an extension of the model was proposed, in which the values of the temperature and baryon chemical potential evolve smoothly with collision energy [32]. The energy dependence of the  $E_S$  ratio calculated within this extended hadron gas model is compared to the experimental results in Fig. 4. By construction, the prevailing trend in the data is reproduced by the model but the decrease of the ratio between 30A and 80A GeV is not well described. The measured strangeness to pion yield in central Pb+Pb collisions at 158A GeV is about 25% lower than the expectation for the fully equilibrated hadron gas [32, 33]. Obviously the non-equilibrium hadron gas models [27, 34, 35] with the parameters fitted separately to the data at each energy describe the experimental results significantly better. Interestingly, it was found in [36] that the transition from baryon to meson dominated freeze-out conditions happens to be located at low SPS energies.

Dynamical models of A+A collisions, such as RQMD [37], UrQMD [39] and HSD [42] treat the initial nucleon-nucleon interactions within a string-hadronic framework. In addition these models include effects such as string-string interactions and hadronic re-scattering which are expected to be relevant in A+A collisions. The predictions of the RQMD [37, 38], UrQMD [39, 40, 41] and HSD [41] models are shown in Figs. 3, 4, 5, 6 and 7. It is seen that all these models, like the hadron gas model, fail to describe the rapid change of the hadron production properties with collision energy in the low SPS energy range. It was recently shown that the maximum in relative strangeness production can be reproduced by invoking an unusually long lifetime of the fireball at low SPS energies which decreases with the collision energy [43]. This assumption is however difficult to justify with the dynamical models of the collision process [39, 42] and the results on the energy dependence of the two-pion correlation function [44]. Finally, the onset of the step-like structure in the energy dependence of the inverse slope parameter of the  $m_T$  spectra can be reproduced within the hydrodynamical model by introduction of a rapid change of the freeze-out conditions at low SPS energies [45]. However, this assumption does not explain the increase of the  $T$ -parameter suggested by the RHIC results. Thus, one can conclude that the models which do not invoke the onset of deconfinement at the low SPS energies can not explain the energy dependence of hadron production properties in central Pb+Pb (Au+Au) collisions.

## SUMMARY

In summary, new results on charged pion and kaon production in central Pb+Pb collisions at 20A and 30A GeV were presented and compared to measurements at lower and higher energies. A change of energy dependence is observed around 30A GeV for the yields of pions and kaons as well as for the shape of the transverse mass spectra. Available model explanations are discussed. At present a reaction scenario with the onset of deconfinement at low SPS energies best reproduces the data.

## Acknowledgments

This work was supported by the US Department of Energy Grant DE-FG03-97ER41020/A000, the Bundesministerium fur Bildung und Forschung, Germany (06F137), the Virtual Institute VI-146 of Helmholtz Gemeinschaft, Germany, the Polish State Committee for Scientific Research (1 P03B 006 30, 1 P03B 097 29, 1 PO3B 121 29, 1 P03B 127 30), the Hungarian Scientific Research Foundation (T032648, T032293, T043514), the Hungarian National Science Foundation, OTKA, (F034707), the Polish-German Foundation, the Korea Science & Engineering Foundation (R01-2005-000-10334-0), Stichting FOM, the Netherlands, the Bulgarian National Science Fund (Ph-09/05) and the Croatian Ministry of Science, Education and Sport (Project 098-0982887-2878).

---

## References

- [1] J. C. Collins and M. J. Perry, Phys. Rev. Lett. **34**, 1353 (1975), E. V. Shuryak, Phys. Rep. **61**, 71 (1980) and **115**, 151 (1984).
- [2] Y. Aoki, Z. Fodor, S. D. Katz and K. K. Szabo, Phys. Lett. B **643**, 46 (2006), M. Cheng *et al.*, Phys. Rev. D **74**, 054507 (2006).
- [3] J. Rafelski and B. Müller, Phys. Rev. Lett. **48**, 1066 (1982), T. Matsui and H. Satz, Phys. Lett. B **178**, 416 (1986).
- [4] M. Gaździcki and D. Röhrlach, Z. Phys. C **65**, 215 (1995); C **71**, 55 (1996) and references therein.
- [5] M. Gaździcki, Z. Phys. C **66**, 659 (1995).
- [6] M. Gaździcki and M. I. Gorenstein, Acta Phys. Polon. B **30**, 2705 (1999) and references therein.
- [7] S. V. Afanasiev *et al.* [The NA49 Collaboration], Phys. Rev. C **66**, 054902 (2002).
- [8] S. Afanasiev *et al.* (NA49 Collab.), Nucl. Instrum. Meth. A **430**, 210 (1999).
- [9] A. Bialas, M. Błeszyński and W. Czyż, Nucl. Phys. B **111**, 461 (1976).
- [10] B. Andersson, G. Gustafson and Hong Pi, Z. Phys. C **57**, 485 (1993).
- [11] for more details on the procedure see: C. Alt *et al.* [The NA49 Collaboration], Phys. Rev. C **73**, 044910 (2006).
- [12] K. Werner, Phys. Rep. **232**, 87 (1993).
- [13] C. Alt *et al.* [The NA49 Collaboration], J. Phys. G: Nucl. Part. Phys. **31**, S685 (2005).
- [14] E. Fermi, Prog. Theor. Phys. **5**, 570 (1950).
- [15] D. Pelte *et al.* [FOPI Collaboration], Z. Phys. A **357**, 215 (1997),  
L. Ahle *et al.* [E802 Collaboration], Phys. Rev. C **57**, 466 (1998),  
L. Ahle *et al.* [E802 Collaboration], Phys. Rev. C **58**, 3523 (1998),  
L. Ahle *et al.* [E802 Collaboration], Phys. Rev. C **60**, 044904 (1999),  
L. Ahle *et al.* [E802 Collaboration], Phys. Rev. C **60**, 064901 (1999),  
L. Ahle *et al.* [E866 and E917 Collaborations], Phys. Lett. B **476**, 1 (2000),  
L. Ahle *et al.* [E866 and E917 Collaborations], Phys. Lett. B **490**, 53 (2000),  
J. Barrette *et al.* [E877 Collaboration], Phys. Rev. C **62**, 024901 (2000),  
J. Klay *et al.* [E895 Collaboration], Phys. Rev. Lett. **88**, 102301 (2002),  
B.B. Back *et al.* [E917 Collaboration], Phys. Rev. C **66**, 054901 (2002),  
J. Klay *et al.* [E895 Collaboration], Phys. Rev. C **68**, 054905 (2003).
- [16] I. G. Bearden *et al.* [BRAHMS Collaboration], Phys. Rev. Lett. **88**, 202301 (2002),  
B. B. Back *et al.* [PHOBOS Collaboration], arXiv:nucl-ex/0301017,  
M. Velkovsky [PHENIX Collaboration], J. Phys. G **30**, S187 (2004),  
C. Adler *et al.* [STAR Collaboration], Phys. Lett. B **595**, 143 (2004),  
S.S. Adler *et al.* [PHENIX Collaboration], Phys. Rev. C **69**, 034909 (2004),  
K. Adcox *et al.* [PHENIX Collaboration], Phys. Rev. C **69**, 024904 (2004),  
J. Adams *et al.* [STAR Collaboration], Phys. Rev. Lett. **92**, 112301 (2004),  
I. G. Bearden *et al.* [BRAHMS Collaboration], Phys. Rev. Lett. **94**, 162301 (2005),  
I. Arsene *et al.* [BRAHMS Collaboration], Phys. Rev. C **72**, 014908 (2005).
- [17] T. Anticic *et al.* [NA49 Collaboration], Phys. Rev. Lett. **93**, 022302 (2004).
- [18] M. K. Mitrofski *et al.* [NA49 Collaboration], J. Phys. G **32**, S43 (2006) [arXiv:nucl-ex/0606004].
- [19] M. Gaździcki and O. Hansen, Nucl. Phys. A **528**, 754 (1991).
- [20] I. Bearden *et al.* [NA44 Collaboration], Phys. Lett. B **471**, 6 (1999).
- [21] M. Kliemant, B. Lungwitz and M. Gazdzicki, Phys. Rev. C **69**, 044903 (2004).
- [22] C. Alt *et al.* [NA49 Collaboration], Phys. Rev. C **73**, 044910 (2006).
- [23] L. D. Landau, Izv. Akad. Nauk SSSR, Ser. Fiz. **17**, 51 (1953).
- [24] L. Van Hove, Phys. Lett. B **118**, 138 (1982).
- [25] M. I. Gorenstein, M. Gazdzicki and K. A. Bugaev, Phys. Lett. B **567**, 175 (2003).
- [26] M. Gazdzicki, M. I. Gorenstein, F. Grassi, Y. Hama, T. Kodama and O. J. Socolowski, Braz. J. Phys. **34**, 322 (2004).
- [27] J. Letessier and J. Rafelski, arXiv:nucl-th/0504028.
- [28] J. K. Nayak, J. e. Alam, P. Roy, A. K. Dutt-Mazumder and B. Mohanty, Acta Phys. Slov. **56**, 27 (2005).
- [29] M. Bleicher, arXiv:hep-ph/0509314.
- [30] S. V. Akkelin and Yu. M. Sinyukov, Phys. Rev. C **73**, 034908 (2006).
- [31] R. Hagedorn, CERN report CERN-TH-7190-94 and Proceedings of NATO Advanced Study Workshop on Hot Hadronic Matter: Theory and Experiment, Divonne-les-Bains, Switzerland, 27 Jun - 1 Jul 1994, edited by J. Letessier, H. Gutbrod and J. Rafelski, [Hot Hadronic Matter, v. **346**, 13 (1994)],  
J. Cleymans and H. Satz, Z. Phys. C **57**, 135 (1993),  
J. Sollfrank, M. Gaździcki, U. Heinz and J. Rafelski, Z. Phys. C **61**, 659 (1994),  
P. Braun-Munzinger, J. Stachel, J. Wessels and N. Xu, Phys. Lett. B **365**, 1 (1996),  
G. D. Yen, M. I. Gorenstein, W. Greiner, S.N. Yang, Phys. Rev. C **56**, 2210 (1997),  
F. Becattini and U. W. Heinz, Z. Phys. C **76**, 269 (1997),

- G. D. Yen and M. I. Gorenstein, Phys. Rev. C **59**, 2788 (1999).
- [32] J. Cleymans and K. Redlich, Phys. Rev. C **60**, 054908 (1999),  
P. Braun-Munzinger et al., Nucl. Phys. A **697**, 902 (2002).
- [33] F. Becattini, M. Ga  dzicki and J. Sollfrank, Eur. Phys. J. C **5**, 143 (1998).
- [34] F. Becattini, M. Gazdzicki, A. Keranen, J. Manninen and R. Stock, Phys. Rev. C **69**, 024905 (2004).
- [35] F. Becattini, J. Manninen and M. Gazdzicki, Phys. Rev. C **73**, 044905 (2006).
- [36] J. Cleymans, H. Oeschler, K. Redlich and S. Wheaton, Phys. Lett. B **615**, 50 (2005).
- [37] H. Sorge, H. Stocker and W. Greiner, Nucl. Phys. A **498**, 567C (1989).
- [38] F. Wang, H. Liu, H. Sorge, N. Xu and J. Yang, Phys. Rev. C **61**, 064904 (2000).
- [39] S. A. Bass *et al.*, Prog. Part. Nucl. Phys. **41**, 225 (1998).
- [40] H. Weber, E. L. Bratkovskaya and H. Stoecker, Phys. Lett. B **545**, 285 (2002).
- [41] E. L. Bratkovskaya *et al.*, Phys. Rev. C **69**, 054907 (2004).
- [42] W. Cassing, E. L. Bratkovskaya and S. Juchem, Nucl. Phys. A **674**, 249 (2000).
- [43] B. Tomasik and E. E. Kolomeitsev, Eur. Phys. J. C **49**, 115 (2007).
- [44] S. Kniege *et al.* [NA49 Collaboration], J. Phys. G **30**, S1073 (2004).
- [45] Yu. B. Ivanov and V. N. Russkikh, arXiv:nucl-th/0607070.